

ARCC Technical Paper for the IARC Mission 9

Masahiro Sato*, Rachel Axten*, Venkatakrishnan Iyer*, and Vitor Valente*
Pennsylvania State University, University Park, PA, 16802

The Autonomous Robotics Competition Club's (ARCC) proposed solution consists of a fixed-wing mother ship, the Sig Rascal 168, and a multirotor daughter ship to replace the communications module on the mast. The fixed wing is used to carry the daughter ship close to the mast, wherein it is deployed from the fixed-wing and proceeds to execute the remainder of the mission, i.e. swapping the communication module on the mast. The multirotor uses the Realsense T265 and D435 tracking and depth cameras to measure the center of the blue plate. Model predictive control (MPC) in combination with an autoregressive (AR) model is used to predict the future mast motion and plan trajectory of the daughter ship to track the blue plate. Robotic hooks from the multirotor attach to the corners of the blue plate to help achieve the required tolerances for the main arm to replace the existing communications module. The multirotor uses a pixhawk flight controller with an onboard computer such as the Jetson Nano/TX2 to achieve the desired autonomy. While the drone performs the main mission, the fixed wing will fly back to the landing location to ensure that the mission objectives are completed in the shortest possible time frame.

I. Introduction

THE Autonomous Robotics Competition Club (ARCC) is a student club at The Pennsylvania State University that participates in various ground and aerial robotics competitions. The club is participating in IARC's ninth mission and details of the proposed solution is presented in this work. The authors are the main participants from the club with the possibility of additional members joining at a later phase.

IARC Mission 9 requirements can be divided into two major categories: mission specific and vehicle specific. While the initial USA venue for the competition was in Virginia, the competition rules have subsequently been changed to allow teams to participate from their respective locations due to the ongoing COVID-19 pandemic. The ARCC team has suitably modified the solution to address the aspects with regard to the venue. Mid-State Regional Airport, near Philipsburgh, Pennsylvania, will serve as flight test and competition site for the team. The system design proposed by the team is explained in the following paragraphs. The venue and vehicle specific requirements are used as input factors in the following system design, and the discussion processes of the system design are summarized in Figure 1.

Mission 9 requires the vehicle to fly back and forth for a distance of 3.2 km and complete the tasks within 9 minutes. Considering the time needed for takeoff, landing, and replacing the communication module (CM) attached to the mast, the vehicle must have an average speed of at least 60 km/h. In addition, there are other requirements such as flight altitude of fewer than 15m and mass of less than 90kg. As a result of the trade-off study, the vehicle's configuration, general shape, and basic guidance sequence can be determined.

The next step is to conduct a trade-off study of an image sensor installed in the vehicle to detect the target. Its detection range error can be estimated. Additionally, a trade-off study of the aircraft control theory to determine the positional error of the vehicle will be conducted. Furthermore, the wind speed expected at the test site and on the date of the competition will be investigated from the past weather database. This allows to set the disturbance response of the vehicle due to gusty winds blowing instantaneously.

From the various trade-off studies and requirements analysis described above, the errors in the positional coordinates of the vehicle and the CM attached to the mast can be estimated. The last step is to design the mechanism of the airframe that can tolerate these errors and summarize the system design of the vehicle. Therefore, the competition requirements to each function required of the vehicle will be allocated.

*Graduate Research Assistant, Aerospace Engineering, 2715 Fox Hill Rd.

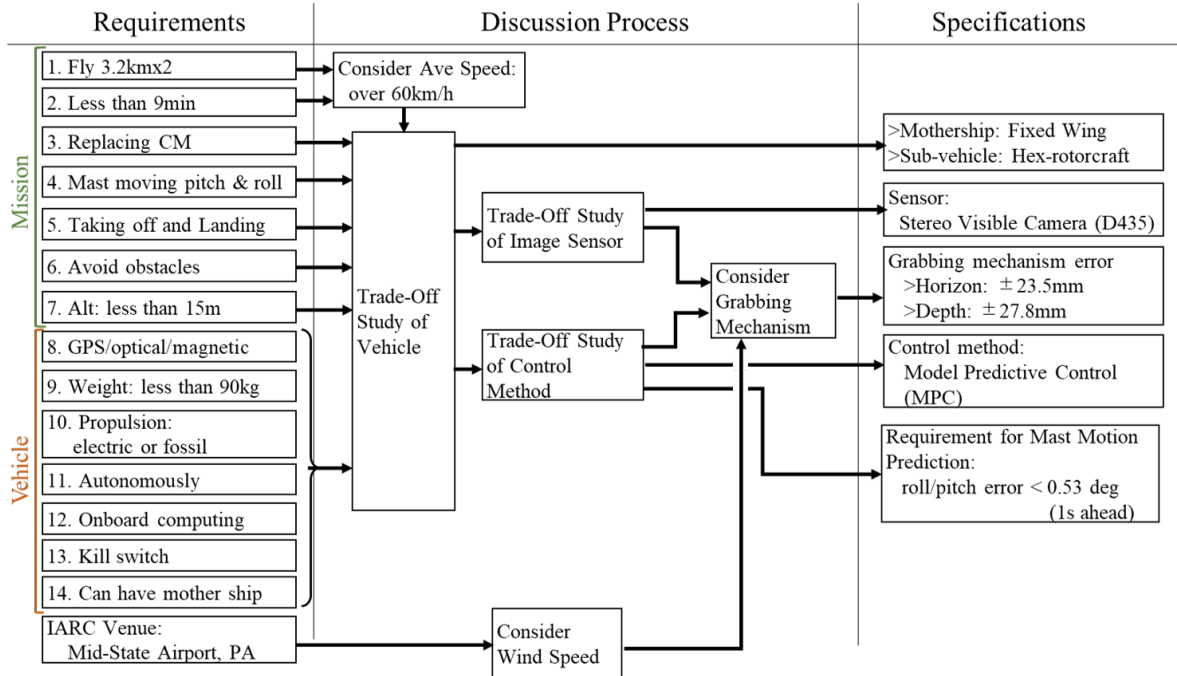


Fig. 1 Discussion processes of the system design for IARC

II. Design Study

A. Vehicle Configuration Trade-off Study

First, a trade-off study of the vehicle based on the requirements is conducted. The result of the trade-off study is shown in Table 1. In this competition, it is possible to operate multiple vehicles, including the mothership and sub-vehicle. There are two viable vehicle proposals: one for single-vehicle operation and the other for multiple-vehicle operation. In multiple aircraft operations, either a helicopter or a fixed-wing aircraft can be candidates for a mothership.



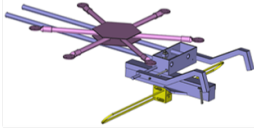

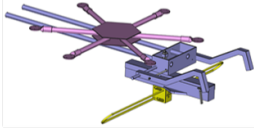
In the case of single-vehicle operation, a relatively sizeable multi-rotor vehicle is considered the best choice since replacing the CM attached to the mast requires hovering due to many obstacles antennas attached to the mast. This multi-rotor vehicle can meet the requirements for maximum speed, weight, and cruising time. However, if the mission is performed by a single aircraft, it is necessary to return to the take-off point after replacing the CM. Thus, there is less time budgeted for replacing the CM in order to land at the take-off point within 9 minutes.

On the other hand, in a multi-vehicle operation, a mothership can return to the take-off point while a sub-vehicle replaces the CM. Therefore, it is easier to accomplish the mission in multi-vehicle operation, allowing sufficient time for the CM replacement operation. As for a mothership, its required task is not so difficult compared to a sub-vehicle, thus it does not matter whether it is a single rotor or a fixed-wing aircraft. However, a helicopter is generally slower, more expensive, and heavier in mass than a fixed-wing aircraft. As a result of the above trade-off study, a fixed-wing aircraft as the mothership and a multi-rotor aircraft is selected as the sub-vehicle.

It is important to note that there is a risk of collision in this multi-vehicle operation with the fixed-wing aircraft when the sub-vehicle is separated from the mother-ship. Computational Fluid Dynamics (CFD) analysis and a wind tunnel test such as the Captive Trajectory System (CTS) test are required for analyzing this issue. Since a wind tunnel test is not feasible due to budget constraints, it is necessary to conduct a simple CFD analysis and step-by-step flight tests. Zipline, a company that delivers medical supplies from an unmanned fixed-wing aircraft capable of flying at 100 km/h, has developed a system to separate parachute-attached cargo by free-falling [1]. Suppose there is a possibility of collision with the mother vehicle in free-fall. In that case, several methods should be tried, such as applying a turning acceleration in the opposite direction in each vehicle at the moment of separation or having the sub-vehicle generate a downward lift force just before separation. This issue is considered as a technical problem to be solved over the course of the competition.

A basic guidance sequence is then considered. Figure 2 shows the results. The mothership carrying the sub-vehicle

Table 1 Trade-off study of vehicles

	Single Vehicle	Multiple Vehicle			
		Helicopter + Multi-rotor		Fixed-wing + Multi-rotor	
Vehicle candidate	AeroRange2 (AGL)	Mothership: Yamaha Rmax	Mothership: Rascal 168		
		 Sub-vehicle: 	 Sub-vehicle: 		
		Mothership	Sub-vehicle	Mothership	Sub-vehicle
Weight (< 90kg)	20kg	94 kg	8 kg	20 kg (Estimated)	8 kg
Average speed (> 60km/h)	60-100 km/h	74 km/h	-	100 km/h (Estimated)	-
Cruising time (> 9min)	100 min	60 min	-	20 min (Estimated)	-
Propulsion	Electric	Fossil fuel	Electric	Electric	Electric
Period to replace CM	2-3 min	1min or less After releasing the sub-vehicle, the mothership can return		1min or less After releasing the sub-vehicle, the mothership can return	
Comprehensive evaluation	Inappropriate	Inappropriate		Appropriate	

makes multiple orbits around the designated pole for a 3.2 km flight. The vehicle will rely on GPS guidance for this portion using waypoints of the pylons known and uploaded to the mission plan before the flight. Moreover, if it is necessary to avoid obstacles, obstacles will be detected using image sensors mounted on the sub-vehicle or the mothership and the path will be recalculated to avoid them. Next, the sub-vehicle is released from the mothership where the image sensor mounted on the sub-vehicle can detect the blue plate of the mast. Since one side of the blue plate is about 350 mm, if the sub-vehicle is equipped with a standard image sensor, the release range for the sub-vehicle is about 5 to 8 meters from the GPS position of the mast. After releasing the sub-vehicle, the mothership returns to the landing point as soon as possible. The sub-vehicle is then guided towards the CM detected from the image without the GPS data. Since the sub-vehicle needs to grab the mast when the CM is replaced, the sub-vehicle needs the relative range information from the mast. Therefore, the sub-vehicle is guided to the CM using image and depth data in its terminal guidance. Finally, the CM is replaced by a mechanism and the sub-vehicle will be left near the mast without returning.

B. Image Sensor

This section will conduct a trade-off study on image sensors that can be installed in the sub-vehicle. Since the sub-vehicle should be as small and light as possible, four candidates for small image sensors are listed according to the detection frequency band. The trade-off results are shown in Table 2. As one of the visible cameras, there is the Raspberry Pi Camera V2, which is the smallest among these candidates, but it is inappropriate because it cannot detect depth data due to a monocular camera. On the other hand, the D435, a visible stereo camera, has sufficient resolution and accuracy of depth data, making it suitable for installation. The L515, which has both a Laser Imaging Detection and Ranging (LiDAR) and a visible camera, can acquire both visible images and depth data. Still, it is designed specifically for indoor use and has a maximum detection range of less than 1 meter outside. A comparison of the images acquired by the D435 and the L515 is shown in Table 3. Therefore, the detection range of the L515 depth data is insufficient and inappropriate. The last IR camera is also inapplicable because it could not acquire depth data, and the blue plate of the target mast is not an object with a heat source.

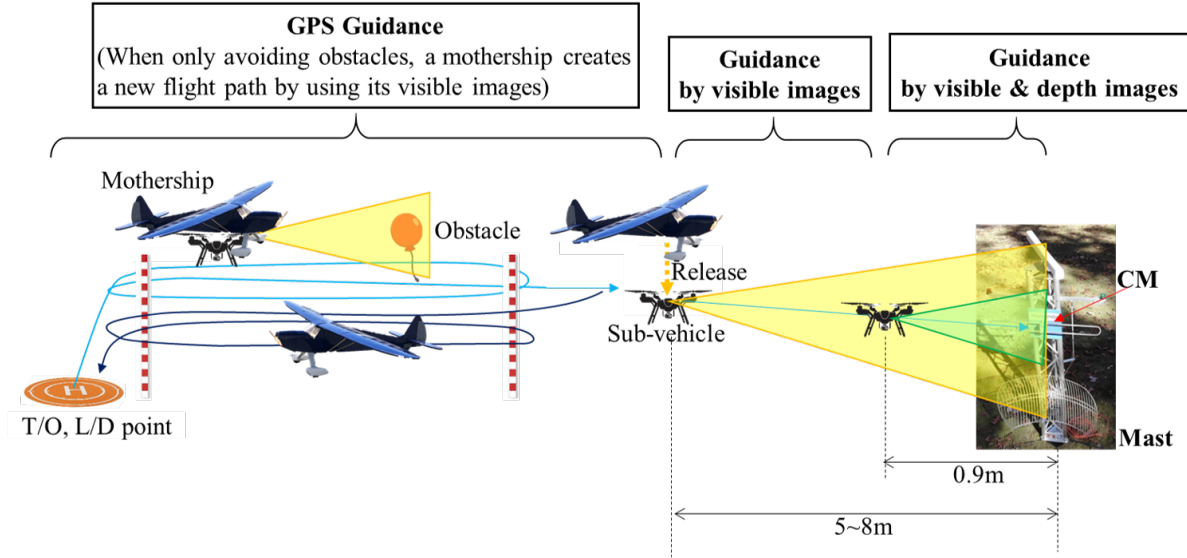







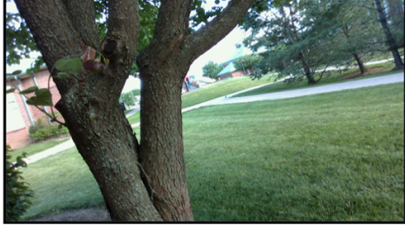
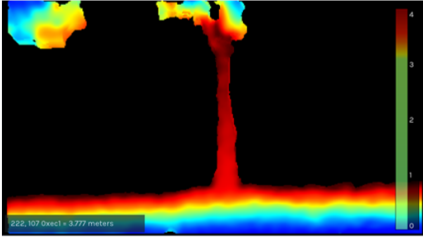
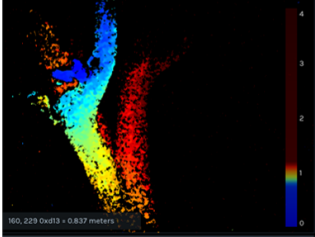
Fig. 2 Basic guidance sequence

Table 2 A trade-off study of image sensors

	Visible (380 - 750nm)		LiDAR (860nm) + Visible	IR (LW:7.5 – 13.5 μ m)
	Mono	Stereo		
Sensor candidate (Example)	Raspberry Pi V2 	D435 	L515 	FLIR Boson 
Pixels	1920 x 1080	1920 x 1080	1024 x 768	640 x 512
FOV [deg]	62.6 x 48.8	69.4 x 42.5	70 x 55 (± 2)	95 (HFOV)
iFOV [deg]	0.037	0.036	0.070	0.190
Frame rate [Hz]	30	30	30	30
Other	-	Range:0.1m-10m Baseline:50mm	Accuracy depends on rider scanning direction	Thermal range:~140 $^{\circ}$ C
Depth error	-	20mm@1m (< 2%)	5mm@1m 14mm@9m	-
Comprehensive evaluation	Depth cannot be measured	Appropriate Depth is measurable. This meets requirements at the close range.	The light one(L515) is optimized at indoor, so the detection range is less than 1m. The heavy one is not suitable due to the weight.	Depth cannot be measured, and resolution is poor

Based on the above trade-off results, the image sensor to be mounted on the sub-vehicle is the D435, a visible stereo camera. The depth data was acquired at different distances to a fixed target to investigate its accuracy as the results are shown in Figure 3. As a result of summarizing the standard deviation of the depth data, it was found that its noise component increased exponentially with range. Therefore, the position data of the target CM shall be collected at a range of 0.9 m, where the blue plate of the mast is sufficiently within the field of view, and the noise is the lowest. The standard deviation of the D435 depth data at 0.9 m will be 4.9 mm.

Table 3 Results of image data captured by D435 and L515

	Stereo (D435)	LiDAR (L515)
Maximum detection range	3.77 m	0.84 m
RGB image		
Depth image		

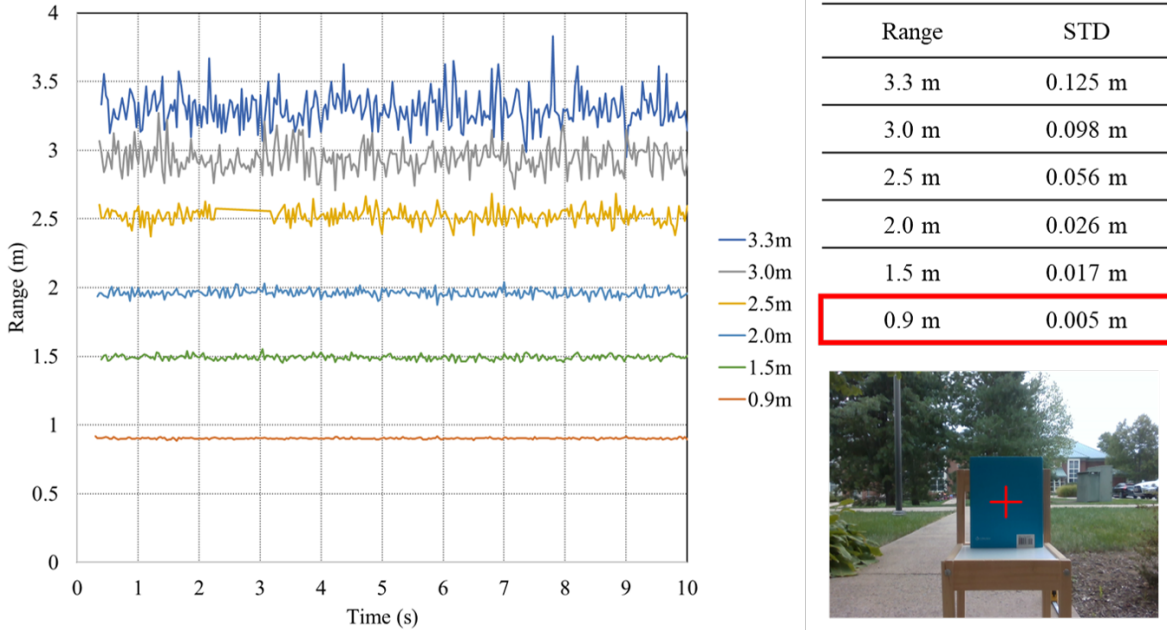


Fig. 3 Depth data noise analysis for a fixed target

III. Mast Motion Prediction

A. Moving Target Detection

The mast mounted on the motion platform was set up outdoors and the proposed image processing algorithm to track the moving blue plate of the mast was tested. The D435 was placed in front of the mast. The target coordinates obtained from the image processing results of the RGB sensor were converted to the roll angle of the mast, and the depth data at the target tracking point obtained from the Stereo sensor was converted to the pitch angle of the mast. An example

of the image processing results of tracking a moving mast on a motion platform using the D435 is shown in Figure 4. Throughout the video, it could be confirmed that the system could track the center coordinates of the blue plate stably. In this test, the roll and pitch angle data entered into the motion platform are compared with those calculated from the D435 sensors. The roll and pitch angles of the motion platform were input with sum of 3 sine wave signals.

During initial testing, the period matches the input data of the motion platform and the actual output result, but the amplitude does not match. This motion platform is a table for a car racing game, and it does not take into account the mounting of an object with a high center of gravity, such as a mast. To check whether the mast attitude angle detected from the image processing is equivalent to the actual mast attitude angle, the angle at which the mast was actually tilted was measured from the RGB images acquired. The result is shown in Figure 5. Comparing the image at 0 seconds, just before the start of the motion, with the image at 65 seconds, when the input command value of the roll angle was 13.7 deg, it was found that the mast was tilted 4 deg to the right. The roll angle calculated by image processing is 5.1 deg, and the pitch angle is -1.6 deg, which is equivalent to the result calculated simply from the images. Therefore, it can be considered that the motion platform is not controlled sufficiently due to backlash and insufficient torque and that the results detected by the image processing are correct. The team will seek to build a new motion platform that is capable of achieving the commanded roll and pitch attitudes for future testing and the competition runs. The data shows that the RGB sensor can detect the roll angle at a range of 3.3m from the mast, but the depth data from the Stereo sensor contains a lot of noise. This indicates that it is necessary to get as close as 0.9m to collect the depth data.

B. Autoregressive model (AR) prediction initial results

The current mast prediction algorithm relies on an AR model to predict the time-series of mast motion one second ahead. It has been studied for a long time in economic indicators such as the unemployment rate and finance and the analysis of stock prices, and numerous applications exist. The system allocation for ship motion prediction is an error of less than ± 0.53 deg from the true value one second ahead. It is necessary to select the number of past data used for prediction and the order of the AR model as small as possible so that the calculation time and the data collection time for future prediction will be as short as possible. In choosing the AR model order, the Akaike information criterion (AIC) and the Bayesian Information Criterion (BIC), which have the prediction accuracy, the model order, and amount of data as the evaluation function, are commonly applied [2]. Since the evaluation criteria are clear, a parametric study is performed on the pitch motion of the SCONE model to determine the optimal AR model order and the number of historical data to be used. Since the ship motion to be predicted is one second ahead, it is needed to predict it by using the 0.5-seconds sampling data of the past position obtained by image processing. After determining the parameters, it is also needed to check if these are valid for other waves.

First, the number of past input data for prediction is set as 100-1000 data points with 0.5-seconds sampling, which means that the length of data needed to make a prediction is 50 to 500 seconds. Furthermore, the AR model order is set to 5%, 10%, 20%, 30%, and 40% of the total input data for each case. Hence, parametric studies on 50 cases will be performed in total. Next, the Root Mean Square (RMS) error of the predicted value and the true value after one second is calculated, then the sum of the mean value and three times the standard deviation for evaluation is applied. Assuming that the RMS error has a variance due to a Gaussian distribution, evaluating this value allows us to keep 99.7% of the results below the system allocation. The result is shown in Figure 6. Here "statsmodels" is applied, which is a Python library that provides classes and functions for exploring statistical data, in the Python 3.7 development environment. The red dots in Figure 6 represent the points where "Average+3 σ " of RMS error is minimized for each input data case. It can be seen that the best number of input data is 200, that is, 100 seconds of data, and the best AR model order is 20, to meet the requirement of the system allocation value of 0.53 deg or less.

The AR model was applied with the above parameters, and the data one second ahead for a total of five input waves are evaluated. The following table 4 shows the RMS error mean, standard deviation (σ), and "Average+3 σ " of RMS error for each case. It is seen that the required distribution value of 0.53 deg or less is satisfied in all cases. Therefore, the AR model with 20th order and 200 previous data input values is applied to predict the movement of the mast one second ahead.

IV. Initial Vehicle Implementation

The following section outlines the initial ARCC vehicle implementation for IARC Mission 9. The full implementation consists of two vehicles: the main vehicle (or mothership) and a subvehicle. The main vehicle is responsible for the long distance flight (or initial part of the mission) from take-off to the point where the mast is located. The second vehicle, once detached from the mothership, will autonomously approach the mast and replace the communication module.

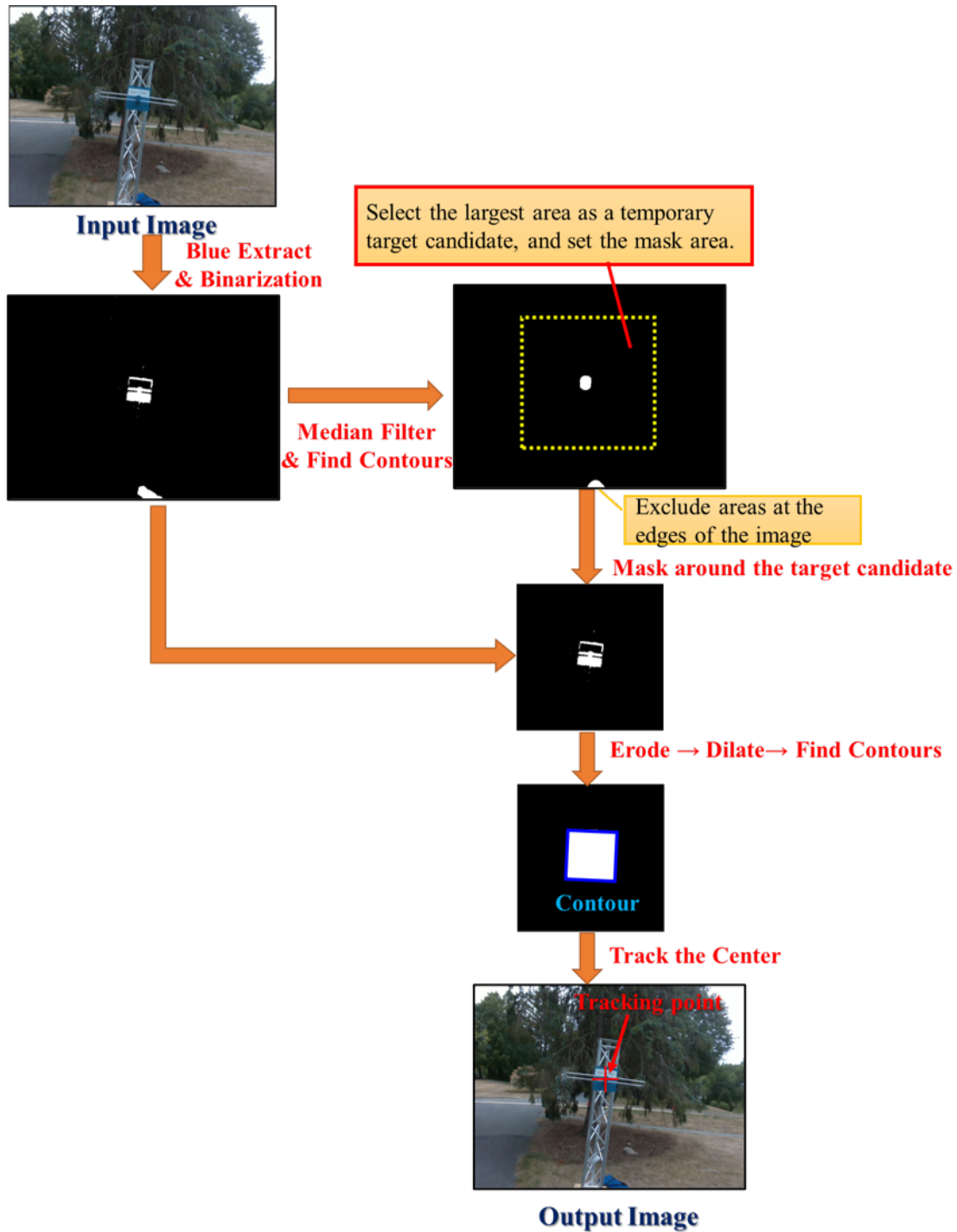


Fig. 4 Example of image processing results of tracking the moving mast on the motion platform using the D435.

A. Subvehicle and CM Replace Mechanism

The subvehicle will be equipped with a Pixhawk flight controller and the PX4 firmware. A companion computer (Jetson Nano/TX2) will be used to perform the desired computations such as target detection, position estimation using the tracking and depth camera data, etc. The companion computer will utilize data from multiple sources with to provide

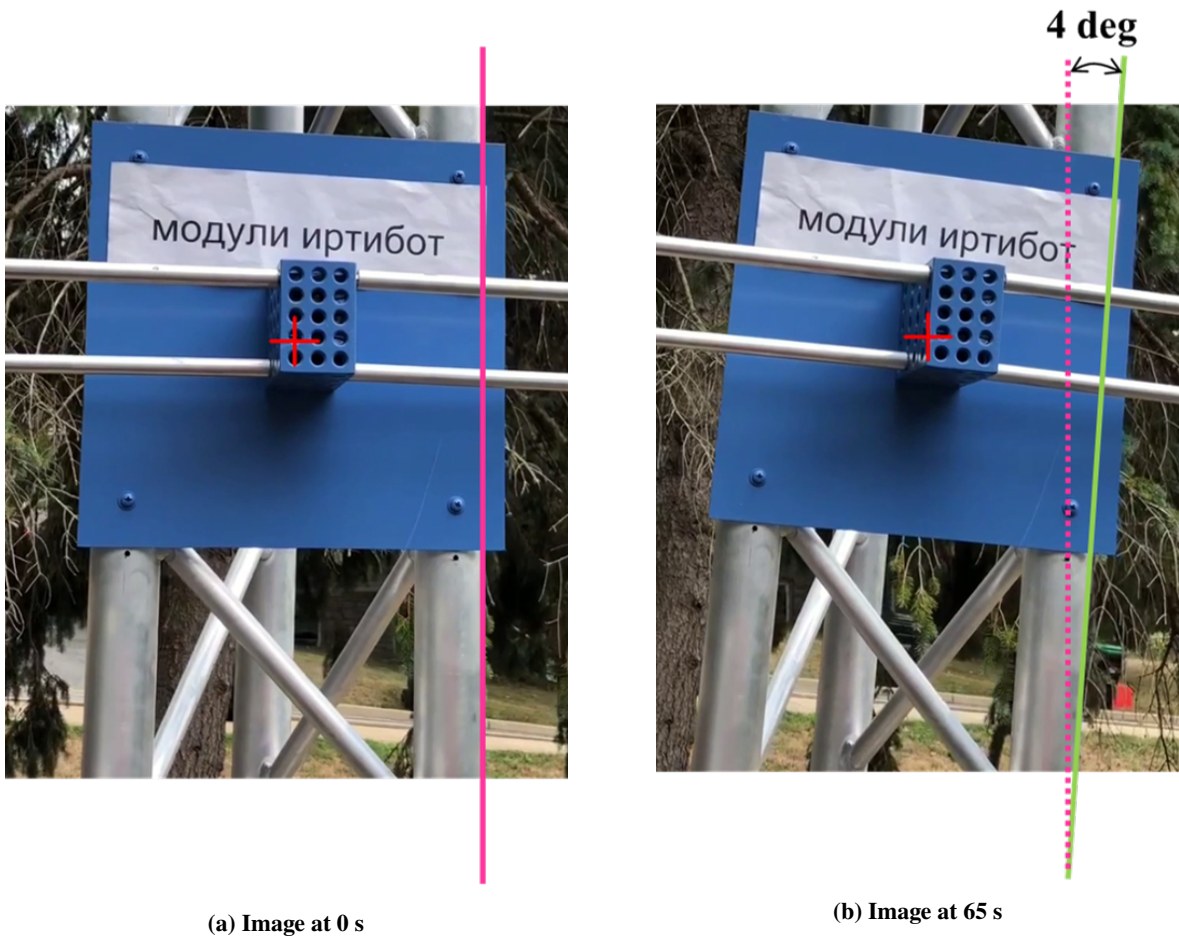


Fig. 5 Measurement results of the angle at which the mast is tilted at the range R=0.9m.

Table 4 RMS error results for 5 input waves

Input wave	RMS error (deg)		
	Average	Standard deviation(σ)	Average+ $3 \times \sigma$
SCONE(Roll)	0.163	0.119	0.520
SCONE(Pitch)	0.031	0.024	0.104
Sum of 3 sine waves	0.000	0.000	0.001
Sum of 5 sine waves	0.002	0.002	0.007
Sum of 10 sine waves	0.001	0.001	0.006

accurate information to the flight controller. The companion computer will also be responsible for handling the mission once the multirotor is released from the fixed wing aircraft. Offboard mode of the PX4 firmware will be engaged and the companion computer will provide position and velocity set-points to the flight controller to navigate to the mast and track the mast motion. To aide the position accuracy of the multirotor, the aircraft will be equipped with a RTK GPS, that in conjunction with the T265 and D435 camera will help achieve the desired level of accuracy.

The subvehicle is presented in the Fig. 7-a. The current configuration is a hexcopter with rotors equally distributed in a circle. This specific configuration was selected based on consideration of design trade-offs and also based on the need of carrying the mechanism to replace the CM. The propulsion system for this vehicle consists of six 6S 380kV brushless motors, running 13" carbon fiber propellers and 40A ESCs. The mechanism that will be used to replace the CM is

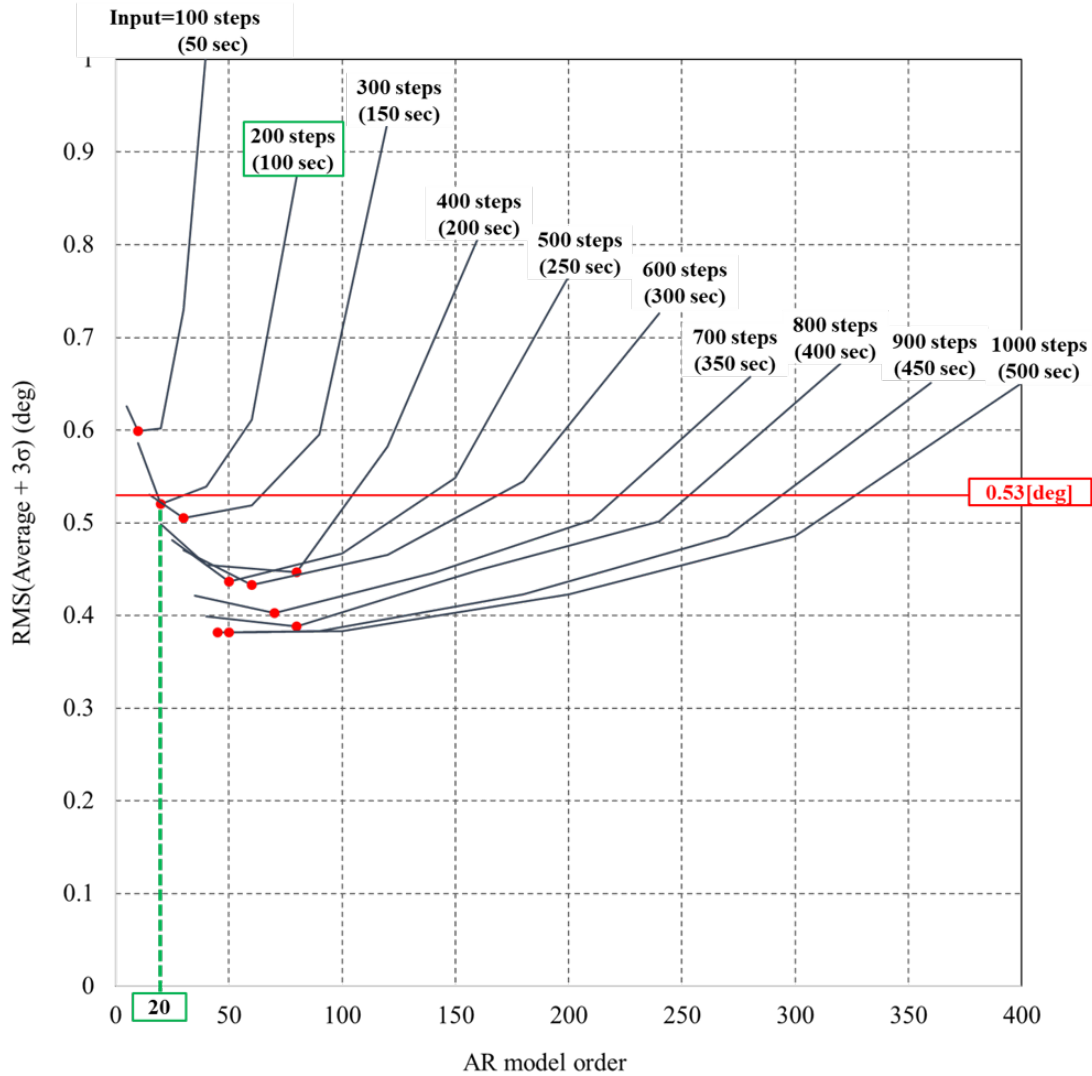


Fig. 6 The result of parametric study on the AR model order and the number of input data

presented in the Fig. 7-b. It consists of a carbon fiber structure that allows a sliding mechanism to operate. The hooking mechanism consists of two hooks that will be deployed once the position is within a specified range. Once hooked, the mechanism will start the sliding phase to remove and replace the CM. This procedure is presented in the Fig. 8.

When the subvehicle replaces the CM, it needs to grab and be fastened to the mast. The current method to fix the vehicle is to hook it to the bar with the navigation lights, which is placed above the blue plate.

First, the error in the relative position between the sub-vehicle and the bar on the mast where the hook is attached is considered. Table 5 summarizes the factors causing the error based on the previous discussion. The errors include the position error of the target mast and the error of the vehicle itself. One of the target position errors is caused by the image sensor of the vehicle. The horizontal error is equal to one pixel of the instantaneous field of view (iFOV) of the visible image, which is ± 0.6 mm at 0.9 m range. On the other hand, in the depth direction, the error is ± 4.9 mm at 0.9 m range.

Other target position errors include reference position errors resulting from the control method, which can result in an error of ± 0.21 degrees for the MPC. The bar on the mast where the sub-vehicle hooks is located about 1.74 m from

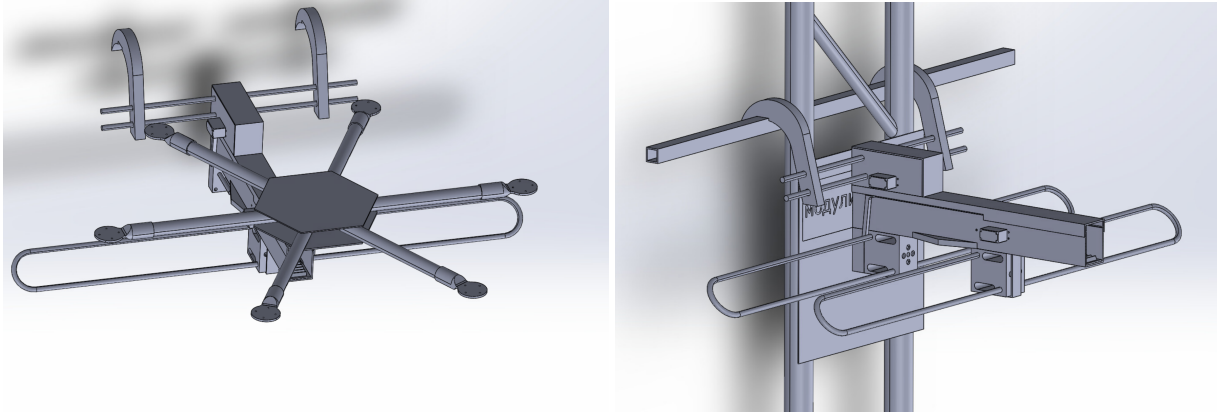


Fig. 7 a) Hexarotor configuration for the subvehicle. b) Current configuration grab and replacing mechanism.

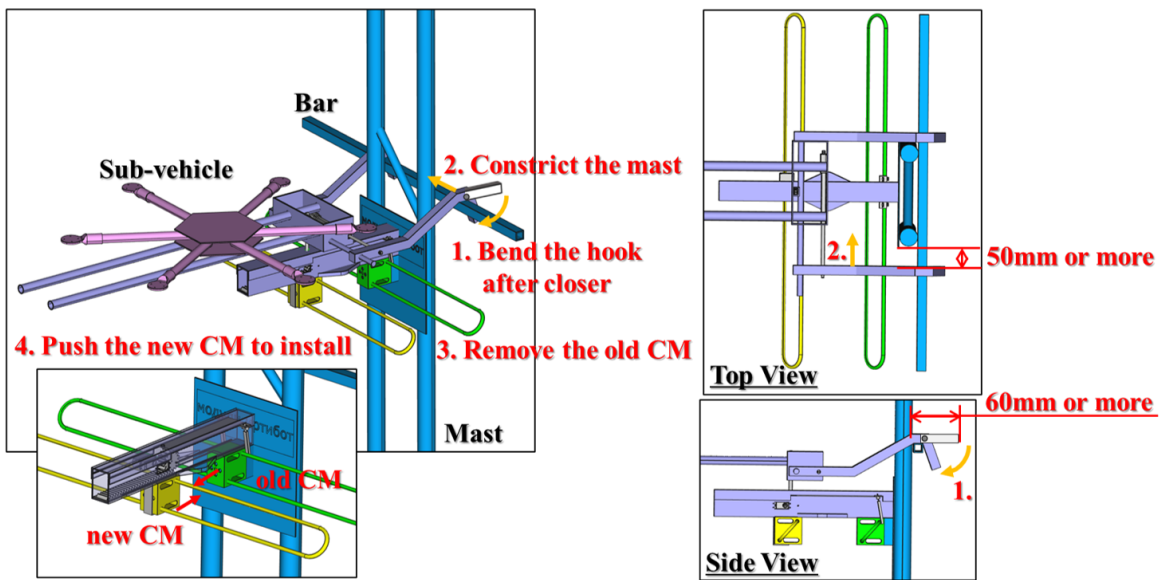


Fig. 8 Mechanism of grabbing the mast.

the mast base, then the error at the bar location is ± 6.4 mm. The angular error assigned to the motion prediction is less than ± 0.53 degrees, then the error at the bar is ± 16.1 mm.

Next, the errors in the subvehicle itself is considered. From consideration of the wind at the planned competition site, the disturbance error due to wind speed is ± 0.4 mm. In addition, it is assumed that the sub-vehicle is equipped with the MPU6000, which is one of the MEMS IMUs. According to the literature [3], the average static bias of the MPU6000 accelerometer is -0.135 m/s² when it is stationary for 1 hour. Therefore, the vehicle has an error of $\pm 6.7 \times 10^{-3}$ m/s² for 0.01 sec, which is one step of the control calculation, and can be considered a negligible error.

By adding up the above assumed errors, the relative error near the bar on the mast is ± 27.1 mm in the horizontal direction and ± 31.4 mm in the depth direction, which is the allowable error of the grabbing mechanism.

Figure 8 shows the design result of the mechanism to exchange the CM by hooking the bar on the mast with these considerations. First, the subvehicle accumulates the trajectory data of the CM position at a distance of 0.9 m from the mast and predicts its future motion. After the prediction, the vehicle approaches the mast by applying MPC. When it gets close enough, it bends the tip of the hook and grabs the bar on the mast. Then, the subvehicle constricts its hooks for fastening itself. Furthermore, the vehicle remove the old CM and insert the new CM into the pins by using the actuator power. To tolerate the relative position error between the bars on the mast and the sub-vehicle, the hook tips before bending shall be at least 65 mm long, and the extra clearance between the two hooks shall be at least 55 mm long.

The results derived from these system designs are summarized in the already shown Figure 1.

Table 5 Tolerance for grabbing mechanism

Error		Horizontal (Y) [mm]	Depth (X) [mm]	Notes
Target Position	Image Sensor	± 0.6	± 4.9	MAX: 0.036[deg] (iFOV@Range 0.9m)
	MPC	± 6.4	± 6.4	MAX: 0.21[deg] (input: SCONE-roll)
	Motion prediction (Requirement)	± 16.1	± 16.1	MAX: 0.53[deg] (1s ahead prediction)
Vehicle Position	Disturbance response (due to wind)	± 0.4	± 0.4	MAX($\pm 3\sigma$): 0.04[m] per 1 sec (1step (=0.01s))
	IMU	$\pm 6.7 \cdot 10^{-3}$	$\pm 6.7 \cdot 10^{-3}$	Static Bias of Accelerometer: -0.135[m/s ²] (1step (=0.01s))
Tolerance For Grabbing Mechanism		± 23.5	± 27.8	

B. Main-vehicle: Rascal 168

In line with the requirements of the competition, complete autonomy will be implemented for both the UAS. The fixed wing aircraft will be equipped with a Pixhawk flight controller running the Ardupilot firmware. Since the location of the two masts are known apriori, standard waypoint navigation can be implemented on the fixed wing with a pre-programmed flight path that the controller will follow. Since the fixed-wing aircraft is just expected to fly the desired distance, release the multicopter and head back to the start location, basic pre-programmed flight plan would suffice without the need for additional autonomy and sensors.



Fig. 9 Rascal 168 Fixed-wing Aircraft for Carrying Subvehicle System to the Mast

The completed aircraft is shown in figure 9 and has conducted initial manual and autonomous waypoint missions.

The desired cruise speed of the mothership vehicle is at least 16.7 m/s (60km/h). Initial manual flight testing has the Rascal 168 model capable of meeting this requirement. Figure 10 shows the vehicle flying at a cruise airspeed of around 20 m/s, with ground speed slightly less due to a headwind. Future testing will verify the cruise speed is maintained above 16.7 m/s when loaded with the subvehicle as required in order to complete the mission in under 9 minutes.

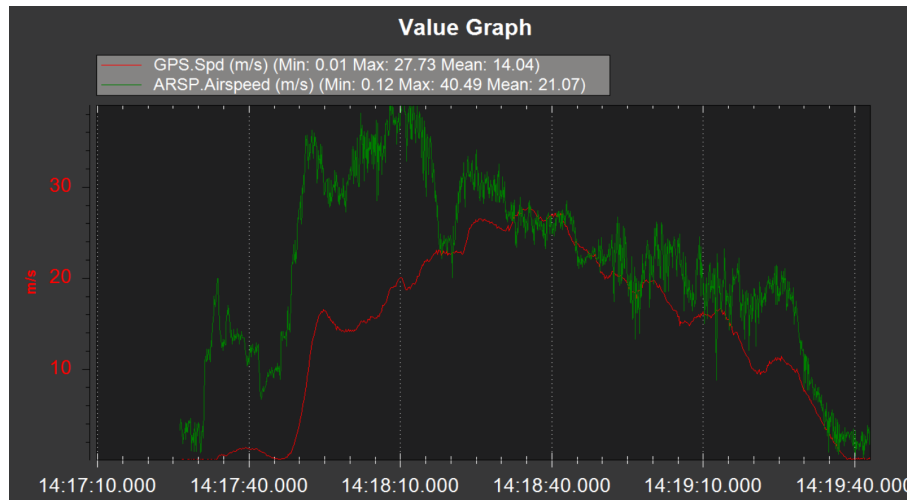


Fig. 10 Rascal 168 Ground Speed vs Airspeed During Initial Flight Testing

V. Conclusion

The Penn State ARCC team has conducted initial work towards vehicle design, flight testing, and mast motion prediction in pursuit of the IARC Mission 9. Future work will seek to integrate mast data with path planning for the subvehicle and flight testing for the mothership and subvehicle combination, including in-air drop tests of the subvehicle.

Acknowledgments

The team thanks Dr. Eric Johnson for his guidance and support as the faculty advisor for ARCC, and Leonard Metkowski for serving as the test pilot for initial flight testing of the Sig Rascal.

V. Valente was partly supported by Instituto Federal de Educação, Ciência e Tecnologia do Rio Grande do Sul - IFRS/Brazil.

References

- [1] Ackerman, E., and Koziol, M., "The blood is here: Zipline's medical delivery drones are changing the game in Rwanda," *IEEE Spectrum*, Vol. 56, No. 5, 2019, pp. 24–31.
- [2] Bishop, C. M., "Pattern recognition," *Machine learning*, Vol. 128, No. 9, 2006.
- [3] Gonzalez, R., and Dabove, P., "Performance assessment of an ultra low-cost inertial measurement unit for ground vehicle navigation," *Sensors*, Vol. 19, No. 18, 2019, p. 3865.